Selective Adsorption of CO2on Zeolites NaK-ZK-4 with Si/Al of 1.8-2.8

ACS OMEGA

http://pubs.acs.org/journal/acsodf

Article

Selective Adsorption of CO_2 on Zeolites NaK-ZK-4 with Si/Al of 1.8–2.8

Ocean Cheung, Zoltán Bacsik, Nicolas Fil, Panagiotis Krokidas, Dariusz Wardecki, and Niklas Hedin*

Cite This: *ACS Omega* 2020, 5, 25371–25380

Read Online

ACCESS | Metrics & More | Article Recommendations | Supporting Information

ABSTRACT: Zeolites with appropriately narrow pore apertures can kinetically enhance the selective adsorption of CO_2 over N_2. Here, we showed that the exchangeable cations (e.g., Na^+ or K^+) on zeolite ZK-4 play an important role in the CO_2 selectivity. Zeolites NaK ZK-4 with Si/Al = 1.8–2.8 had very high CO_2 selectivity when an intermediate number of the exchangeable cations were K^+ (the rest being Na^+). Zeolites NaK ZK-4 with Si/Al = 1.8 had high CO_2 uptake capacity and very high CO_2-over-N_2 selectivity (1190). Zeolite NaK ZK-4 with Si/Al = 2.3 and 2.8 also had enhanced CO_2 selectivity with an intermediate number of K^+ cations. The high CO_2 selectivity was related to the K^+ cation in the 8-rings of the α-cage, together with Na^+ cations in the 6-ring, obstructing the diffusion of N_2 throughout the zeolite. The positions of the K^+ cation in the 8-ring moved slightly (max 0.2 Å) toward the center of the α-cage upon the adsorption of CO_2, as revealed by in situ X-ray diffraction. The CO_2-over-N_2 selectivity was somewhat reduced when the number of K^+ cations approached 100%. This was possibly due to the shift in the K^+ cation positions in the 8-ring when the number of Na^+ was going toward 0%, allowing N_2 diffusion through the 8-ring. According to in situ infrared spectroscopy, the amount of chemisorbed CO_2 was reduced on zeolite ZK-4s with increasing Si/Al ratio. In the context of potential applications, a kinetically enhanced selection of CO_2 could be relevant for applications in carbon capture and bio- and natural gas upgrading.

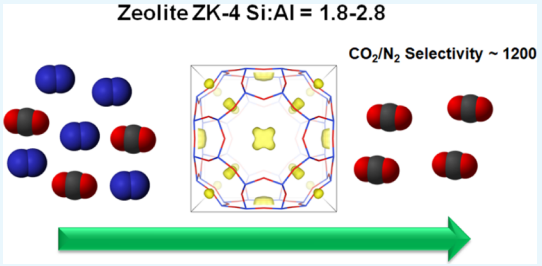

INTRODUCTION

The increasing level of CO_2 in the atmosphere has often been linked to the climate change experienced in recent years. A possible strategy to limit global warming to well below the 2 °C[1] is carbon capture and storage (CCS). CCS has however not been implemented at scale partly because of legislative and economic reasons and public perception. One of the main challenges with its implementation is in the energy penalty and the cost in capturing the CO_2 at point sources of emissions. On the other hand, amine scrubbers are well-developed technically and are used to remove CO_2 from various gas mixtures in some industries. Unfortunately, CO_2 removal by chemical reactions in solutions with amines is associated with a significant energy use during regeneration.[2] Hence, different means to capture CO_2 from gas mixtures, such as postcombustion CO_2 capture using swing adsorption technologies,[3] are being investigated.

Adsorption-based CO_2 capture can be built to operate at different temperatures.[4] A low-temperature setup is considered as the most convenient to install at point sources such as power plants, cement industries, and pulp mills. Adsorption-based technologies require a suitable adsorbent for efficient operation. A suitable solid adsorbent for the separation of CO_2 from gas mixtures would rapidly capture CO_2 with high capacity and selectivity. Furthermore, the adsorbents would have a relatively low heat of adsorption, long lifetime, low costs, and so forth.[3] Chemisorbents such as amine-modified sorbents[5] are being studied. Physisorbents such as zeolites,[6] carbons,[7] phosphates,[8,9] and porous coordination polymers including metal–organic frameworks[10] and zeolitic imidazolate frameworks[10] are also being investigated as potential CO_2 adsorbents.

Zeolites are microporous (with pores up to two nm in diameter, according to the IUPAC) crystalline aluminosilicates, which are negatively charged because of the lack of the charge balance from the +3 oxidation state of Al (with the oxidation state of Si being +4). The negative charge is instead balanced by exchangeable cations. There are many zeolites that have been tested as CO_2 adsorbents.[6,11] Zeolites with large pore apertures that are encircled by 10 or 12 oxygen atoms individually bridged by a silicon or aluminum atom (known as 10- and 12-rings, respectively) typically have a large uptake of CO_2 and a comparably low N_2 uptake at low pressures. As CO_2 has a lower saturation pressure (at a given temperature) and higher electrical quadrupole moment than N_2, CO_2 is preferably physisorbed on porous materials. This effect from the electrical quadrupole moment of CO_2 is observed

Received: August 5, 2020
Accepted: September 11, 2020
Published: September 25, 2020

Table 1. Number of Na^+ and K^+ Ions in the Unit Cells of Zeolite Na-ZK-4 with Different Si/Al Ratios, Estimated Population of the 6- and 8-Ring Windows, CO_2 and N_2 Uptake Levels and Limiting Henry's Law Values, and CO_2-over-N_2 Selectivity[a]

Na/K atomic ratio (ICP−OES)	number of Na^+ cation	number of K^+ cation	expected 8-ring site occupancy	expected 6-ring site occupancy	CO_2 uptake at 101 kPa (mmol/g)	N_2 uptake at 101 kPa (mmol/g)	Henry's law constant (CO_2) (mmol/g·kPa)	Henry's law constant (N_2) (mmol/g·kPa)	CO_2/N_2 selectivity
				Si/Al = 1.8					
100:0	8.57	0	0.57 Na^+	8 Na^+	4.59	0.584	0.2438	0.005750	42
90:10	7.71	0.86	0.57 Na^+, 0.86 K^+	7.14 Na^+	4.48	0.237	0.2354	0.002350	100
72:28	6.17	2.40	0.57 Na^+, 2.40 K^+	5.60 Na^+	4.45	0.065	0.2924	0.000621	471
63:37	5.40	3.17	3 K^+	5.40 Na^+, 0.17 K^+	4.31	0.025	0.2832	0.000238	1190
49:51	4.20	4.37	3 K^+	4.20 Na^+, 1.37 K^+	3.68	0.025	0.2446	0.000243	1006
32:68	2.74	5.83	3 K^+	2.74 Na^+, 2.83 K^+	3.22	0.042	0.1861	0.000414	450
9:91	0.77	7.80	3 K^+	0.77 Na^+, 4.80 K^+	2.30	0.057	0.1252	0.000578	217
				Si/Al = 2.3					
100:0	7.27	0	0	7.57 Na^+	4.86	0.522	0.2399	0.004870	49
77:23	5.60	1.67	1.67 K^+	5.60 Na^+	4.62	0.404	0.2280	0.003820	60
55:45	4.00	3.27	3.00 K^+	4.00 Na^+, 0.27 K^+	4.46	0.100	0.3390	0.001110	305
48:52	3.49	3.78	3.00 K^+	3.49 Na^+, 0.78 K^+	4.52	0.042	0.3317	0.000456	727
33:66	2.40	4.87	3.00 K^+	2.40 Na^+, 1.87 K^+	4.18	0.075	0.2507	0.000854	294
1:99	0.07	7.20	3.00 K^+	0.07 Na^+, 4.20 K^+	3.41	0.210	0.1936	0.002590	75
				Si/Al = 2.8					
100:0	6.32	0	0	6.32 Na^+	4.46	0.494	0.2611	0.004890	53
76:24	4.80	1.52	1.52 K^+	4.80 Na^+	4.31	0.269	0.2526	0.002620	96
62:38	3.92	2.40	2.40 K^+	3.92 Na^+	4.21	0.079	0.2926	0.000786	372
45:55	2.84	3.48	3.00 K^+	2.84 Na^+, 0.48 K^+	4.04	0.065	0.2782	0.000581	479
23:77	1.45	4.87	3.00 K^+	1.45 Na^+, 1.87 K^+	3.82	0.185	0.2635	0.001830	144
0:100	0	6.32	3.00 K^+	3.32 K^+	3.52	0.221	0.2173	0.002250	97

[a]Adsorption experiments were performed at 273 K.

especially on cation-rich zeolites, such as zeolite X,[12] which was found to have high capacity for CO_2 even at low pressures of CO_2. Cation-rich zeolites have large internal electrical field gradients that interact favorably with the charge distribution of CO_2. Zeolite Y and the cation-poor zeolite ZSM-5 both have fewer cations than zeolite X but have also been studied for CO_2 capture.[11,12] Even with a relatively low number of cations, zeolite ZSM-5 may have advantages as a sorbent for CO_2 capture processes. Zeolite ZSM-5 is significantly less-hydrophilic than both zeolites X and Y. Low hydrophilicity of the adsorbent can reduce the costs of drying the flue gas before the CO_2 capture process.

Small-pore zeolites have 8-ring pore apertures with similar dimensions as small gas molecules. These zeolites have been investigated as adsorbents for CO_2 capture.[13−17] The cation-rich zeolite A may be relevant as they show promising CO_2 adsorption properties and bear a low production cost. Specifically, zeolite A in its Na^+ (4A), Mg^{2+} and Ca^{2+} (5A), and mix-cation NaK-A form have been studied for CO_2 capture.[13,18−21] We have shown that zeolite NaK-A could effectively separate CO_2 from N_2 when the number of K^+ cations was about ∼17 at. % of the total number of cations (the rest being Na^+).[20,22−25] This K^+-controlled selectivity was due to Na^+ being selectively replaced by K^+ in the 8-ring apertures in the α-cage. The K^+ in the 8-ring can effectively hinder the diffusion of N_2 in zeolite NaK-A when a sufficient number of pores are being blocked by K^+.

We also found that the highly selective zeolite NaK-A adsorbent could rapidly take up CO_2 irrespectively of the particle size, which was indicative of transport resistance at the interfaces of small zeolite particles.[23] We further showed that the related mix-cation zeolite NaK ZK-4 (Si/Al = 1.3) had similarly high CO_2 selectivity.[26] This selectivity was also related to that K^+ selectively replaced Na^+ in the 8-ring apertures.

Other types of 8-ring zeolites have been studied with respect to their CO_2 adsorption capacity and CO_2 over N_2 selectivity. These studies have included investigations of the CO_2 adsorption on zeolites chabazite,[27,28] ZK-5,[29] RHO,[15,30] ZSM-25,[17,31] and other compositions.[32,33] For many of these compositions, an enhanced CO_2 selectivity has been observed and related to thermally controlled gating/movement of cations in the zeolites or flexibility in the framework.[16,30] In this study, we turned to zeolite NaK-ZK-4 with a high Si/Al ratio and studied its CO_2 adsorption and estimated its selectivity.

RESULTS AND DISCUSSION

CO_2 and N_2 Uptake of Zeolites Na-ZK-4 and NaK-ZK-4. Zeolites Na-ZK-4 (1.8, 2.3, and 2.8) synthesized in this

https://dx.doi.org/10.1021/acsomega.0c03749
ACS Omega 2020, 5, 25371−25380

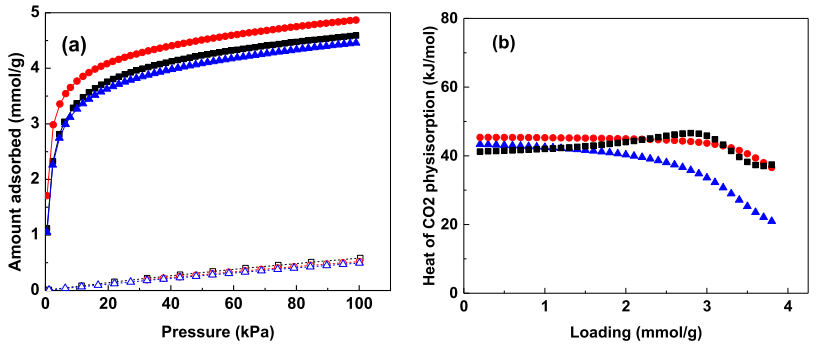

Figure 1. (a) CO_2 (solid symbols) and N_2 (hollow symbols) adsorption isotherms for (■) zeolite Na-ZK-4 (1.8), (●) Na-ZK-4 (2.3), and (▲) Na-ZK-4 (2.8) determined at 273 K. (b) Corresponding loading-dependent heat of CO_2 physisorption.

study were all highly crystalline (Figures S1−S3) with a cubic morphology (Figures S4 and S5) and had all high uptake of CO_2 at 273 K as is detailed in Table 1. The highest CO_2 uptake of 4.86 mmol/g (101 kPa, 273 K) was observed on zeolite Na-ZK-4 (2.3), but comparable levels were observed on zeolites Na-ZK-4 (1.8) (4.59 mmol/g) and Na-ZK-4 (2.8) (4.46 mmol/g). For comparison, zeolite Na-ZK-4 (1.3) and zeolite A (Si/Al = 1:1) showed a CO_2 uptake of 4.35 and 4.21 mmol/g, respectively.[26] Adsorbents with high capacity and selectivity for adsorption of CO_2 are currently being investigated for applications in adsorption-driven separation of CO_2 from the flue gas. An adsorbent with a particularly high CO_2-over-N_2 selectivity and high capacity was tested here. Zeolite ZK-4 (Si/Al ∼ 1.3:1), which had the same structure as zeolite A (LTA), showed a high CO_2 capacity of 4.85 mmol/g (273 K, 101 kPa) in its Na^+ form. When approximately 26 at. % of the extraframework cations were exchanged for K^+ (NaK-ZK-4), the material still adsorbed a large amount of CO_2 (4.35 mmol/g, 273 K, 101 kPa), but the N_2 uptake became negligible (<0.03 mmol/g, 273 K, 101 kPa). The majority of the CO_2 was physisorbed on zeolite ZK-4 as quantified by consecutive volumetric adsorption measurements. The rate of physisorption of CO_2 was fast, even for the highly selective sample. The molecular details of the sorption of CO_2 were revealed as well. Computer modeling (Monte Carlo, molecular dynamics simulations, and quantum chemical calculations) allowed us to partly predict the behavior of the fully K^+-exchanged zeolite K-ZK-4 upon adsorption of CO_2 and N_2 for Si/Al ratios up to 4:1. Zeolite K-ZK-4 with Si/Al ratios below 2.5:1 restricted the diffusion of CO_2 and N_2 across the cages. These simulations could not probe the delicate details of the molecular sieving of CO_2 over N_2. Still, this study indicates that zeolites NaK-ZK-4 and K-ZK-4 could be appealing adsorbents with high CO_2 uptake (∼4 mmol/g, 101 kPa, 273 K) and a kinetically enhanced CO_2-over-N_2 selectivity.[23] We note here that the differences in the CO_2 uptake between these three samples could be related to the differences in the molecular weight of the different zeolites (because of the changes in the number of exchangeable cations). The CO_2 uptake (molecules) per unit cell is listed in Table S1. Unfortunately, the changes in the molecular weight of the zeolite alone could not explain the trend observed. We therefore speculate that the differences were probably also related to the crystallinity of zeolite Na-ZK-4 (the calcination could have affected the crystallinity of the zeolites differently). The comparably high CO_2 uptake on the Na-forms of zeolite ZK-4s was related to the absence of the K^+ cations. K^+ is larger and occupies more space, which reduced the pore volume being available for the CO_2 sorption. The CO_2 and N_2 adsorption isotherms for zeolite Na-ZK-4 (1.8, 2.3, and 2.8) recorded at 273 K are displayed in Figure 1. CO_2 and N_2 adsorption isotherms of all samples listed here can be found in the Supporting Information (Figures S7−S12).

In the structure of zeolites Na-ZK-4 (1.8, 2.3, and 2.8), there is one Na^+ cation that is located close to the edge of the 8-ring window.[34,35] As a consequence, the small size of Na^+ appears to allow for noticeable amounts of N_2 to diffuse through the window and be adsorbed within the pores of zeolites Na-ZK-4 (1.8−2.8). In this context, it is worthwhile noting that from a strictly geometric perspective, neither CO_2 nor N_2 would be able to diffuse through an 8-ring window unless there is some concerted movement of the cations. The initial slopes of the CO_2 adsorption isotherm (Henry's law coefficient K_{CO_2}—Table 1) were 0.244 mmol/g/kPa for Na-ZK-4 (1.8), 0.240 mmol/g/kPa for Na-ZK-4 (2.3), and 0.261 mmol/g/kPa for Na-ZK-4 (2.8). These values were significantly smaller than those for zeolite NaA (5.92 mol/g/kPa), and are likely to be related to the relatively large amount of chemisorption of CO_2 observed on the pure zeolite NaA.[36] The pressure- and temperature-dependent CO_2 physisorption isotherms are shown in the Supporting Information (Figures S13−S15). The isosteric heat of CO_2 physisorption calculated using the Clausius−Clapeyron equation is presented in Figure 1b.

The CO_2 heats of adsorption, Q_{st} (CO_2), presented in Figure 1b were determined from the isotherms presented in Figure S13−S15 using the Clausius−Clapeyron equation. The values were ∼40−45 kJ/mol for all samples (up to ∼1.3 mmol/g loading) and within the range estimated optimal for CO_2 removal from the flue gas by temperature, hybrid temperature/pressure, or vacuum swing adsorption.[37]

In our earlier studies, we have observed that on both zeolite NaKA and NaZK-4 (1.3), the K^+ ions would selectively occupy the cation site at the 8-rings.[20,26] When the number of K^+ reached 17 and 26 at. % of the total number of cations, the partial presence of K^+ in the 8-rings would effectively block N_2 from adsorption at 273 K and higher temperatures. The restricted N_2 adsorption observed on zeolite A and ZK-4 (1.3) when the K^+ cation reached a certain at. % was also observed here for zeolite NaK-ZK-4 (1.8). Table 1 shows the expected average number of K^+ and Na^+ that occupied the cation positions in the 6- and 8-rings. Several assumptions regarding the population of the cation sites can be made according to previous studies: (1) when Na^+ is exchanged for K^+, K^+ cations would replace Na^+ in the 8-rings first and then in the 6-rings and (2) the 4-ring cation sites are basically nonpopulated. As can be seen from Table 1 and Figure 2, the N_2 adsorption was

https://dx.doi.org/10.1021/acsomega.0c03749
ACS Omega 2020, 5, 25371−25380

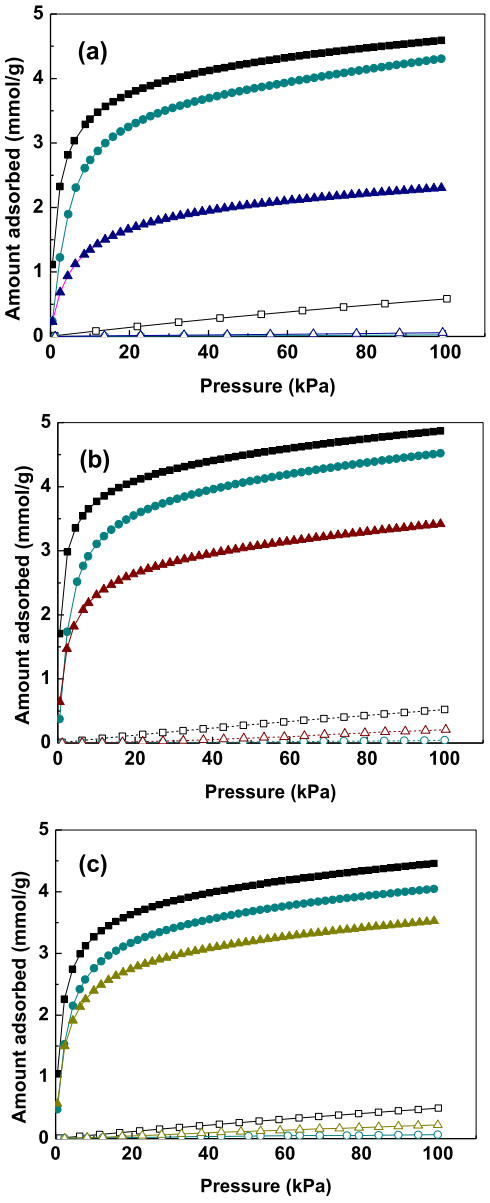

Figure 2. CO_2 (solid symbols) and N_2 (hollow symbols) adsorption isotherms measured at 273 K. (a) Curves for zeolite NaK-ZK-4 (1.8) with cationic fractions of K^+ of 0 at % (■), 37 at.% (●), and 91 at. % (▲), (b) curves for zeolite NaK-ZK-4 (2.3) with cationic fractions of K^+ of 0 at. % (■), 52 at.% (●), and 99 at % (▲), and (c) curves for zeolite NaK-ZK-4 (2.8) with cationic fractions of K^+ of 0 at. % (■), 55 at. % (●), and 100 at. % (▲).

blocked for zeolite NaK-ZK-4 (1.8) with the number of K^+ cations above 28 at. % of K^+ cations correspond to an expected 8-ring occupancy of 0.57 Na^+ + 2.40 K^+. The expected occupancy is consistent with a crystallographic study.[38] For zeolite NaK-ZK-4 with Si/Al = 2.3 and 2.8, similar trends of the adsorption of CO_2 and N_2 were observed as for the sample with Si/Al = 1.8. The amount of N_2 adsorbed first decreased with an increased at. % of K^+. When the number of K^+ reached about ∼50−60 at. %, the N_2 uptake was reduced to close to zero (Table 1 and Figure 2).

The CO_2-over-N_2 selectivity of zeolites can either be measured directly or estimated from the single-component adsorption isotherms of N_2 and CO_2. Ideally, the equilibrium binary adsorption isotherms should be measured to determine the adsorption selectivity; estimation of the adsorption selectivity from single-component adsorption is commonly applied. These estimations always rely on various models. Commonly used ideal adsorbed solution theory (IAST) has complications for zeolites and gas pairs with significantly different adsorption affinities, such as CO_2 and N_2.[39] In addition, it is seldom recognized that the IAST model is not physically self-consistent when for adsorbents with negligible N_2 adsorption as the N_2 adsorption has to be estimated for unphysical high pressures.[40] The Henry's law model used in this study (the CO_2-over-N_2 selectivity listed in Table 1) is more robust than IAST but has obvious limitations in the pressure range, and the results should be treated with care when being extrapolated to the pressures relevant for real adsorption separation processes. The highest CO_2 selectivity was observed for zeolite NaK-ZK-4 with an intermediate number of K^+ cations, irrespectively to the Si/Al ratio. On zeolite NaK-ZK-4 with high CO_2 selectivity, the K^+ cations occupied the 8-ring cation sites but the 6-ring sites were mostly occupied by Na^+; compare with Table 1. This cation configuration resulted in a significantly reduced N_2 adsorption but CO_2 adsorption was not affected in the same way. The CO_2 uptake was still high especially at low pressures. Furthermore, the overall CO_2 uptake (i.e., at 100 kPa) on the zeolites NaK-ZK-4 decreased consistently with the K^+ content. This decrease was related to the large K^+ cation and its larger polarizability than Na^+, which in turn reduced the electric field gradients around the K^+-based CO_2 adsorption sites.

The restricted uptake of N_2 for all of the zeolites NaK-ZK-4 (1.8, 2.3, and 2.8) at an intermediate number of K^+ meant that the CO_2-over-N_2 selectivity had corresponding maxima. We tentatively ascribed this maximum selectivity as an effect of the specific cation composition around the 8-ring of zeolite NaK-ZK-4. The cations around the 6-ring and the 8-ring have the ability to regulate the diffusion of N_2 through the 8-ring. The close-to-zero adsorption of N_2 for the zeolites with an intermediate number of K^+ cations (see Table 1) was ascribed to an effectively blocked diffusion of N_2 because of the comparatively large K^+ cations at a cation site in the 8-ring. As shown in Table 1 and Figure 2, N_2 adsorption could take place when the level of K^+ was further increased. The N_2 adsorption on these NaK-ZK-4s was ascribed to the specific differences of the positions of Na^+ and K^+ in the 6-rings. For zeolite ZK-4[34,35,38] and zeolite A[41] and the Na^+ ions, this 6-ring cation site is placed in the very aperture of the 6-rings but for the K^+ ions, this 6-ring cation site is split into two crystallographic positions on each side of the 6-ring. Because of the fact mentioned above, we expect that with significantly many nonpopulated 6-ring sites (at high Si/Al ratios), the K^+ would move more readily than in compositions with low Si/Al ratios. This expectation is supported by the literature data that have shown high thermal factors (so-called B factors) for the K^+ cations located at the 8-rings on zeolite NaK-ZK-4 at high Si/Al ratios.[38] In short, X-ray diffraction (XRD) findings give extra rationale to the fact that the K^+ in the 8-ring sites is rattling more freely on increasing the level of K^+ for zeolite NaK-ZK-4 at high Si/Al ratios, which in turn opens up for a measurable degree of N_2 adsorption at a high content of K^+. [For this zeolite NaK-ZK-4 (2.8), the CO_2 adsorption capacity was reduced less significantly with respect to the level of K^+ when being compared to zeolite NaK-ZK-4 (1.8)].

https://dx.doi.org/10.1021/acsomega.0c03749
ACS Omega 2020, 5, 25371−25380

It is notable that some diffusion limitations were observed for the pure-Na^+ zeolites ZK-4 at liquid N_2 temperature (77 K). The Langmuir surface areas (recorded at 77 K with N_2, Table S1) showed that a sufficiently rapid N_2 diffusion in zeolite Na-ZK-4 (2.3 and 2.8) was possible but that the diffusion of N_2 in zeolite Na-ZK-4 (1.8) was partly restricted. Note that the cations in the 8-rings of zeolite ZK-4 need in general to move slightly (temporarily or otherwise) to let the CO_2 or N_2 gas to percolate throughout the zeolite; hence, temperature dependency is expected as has been shown by, for example, Shang et al. for chabazite zeolites.[16]

Refinements of the Structures of Zeolite Na-ZK-4 as a Function of Adsorbed CO_2. There is an ongoing discussion on the structural details of 8-ring zeolites and how those relate to the trapdoor, swing door, potential gating of the CO_2 adsorption, and framework flexibility.[14,15,15,16,42,43] We recently deduced from in situ XRD experiments that the cations of zeolite NaK-A did not redistribute upon CO_2 adsorption but instead were slightly displaced toward the center of the α-cage. Here, we performed a similar in situ X-ray diffraction study to investigate the cation position in zeolite K-ZK-4 upon CO_2 adsorption and the positioning of the CO_2 molecules upon adsorption.

For the analysis of the cation distributions in the activated zeolite K-ZK-4 without CO_2 being adsorbed, the XRD data were used to derive a difference electron density (also called as a Fourier map) map. In the Fourier map, only the framework atoms were included so it was possible to observe directly the K^+ positions in zeolite K-ZK-4 (shown by the yellow areas in Figure 3). The map shows significant electron densities in the

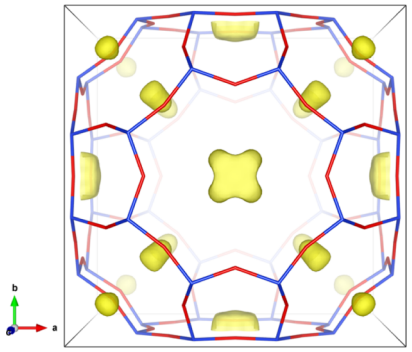

Figure 3. Difference Fourier map (electron densities) and the unit cell with the framework atoms of the dehydrated zeolite K-ZK-4. The yellow areas in the map denote symmetry-related positions of the K^+.

positions on the both sides of the 6-rings and in 8-rings of the structure. These findings are in agreement with prior studies[34,35] (more details of the approach used were presented in our earlier study of zeolite NaKCs-A[44]).

The positional K^+ shift on the adsorption of CO_2 was visualized and determined by a Fourier map using only framework atoms (see Figure 4a), and the K^+ cations shifted along the body diagonal toward the center of the unit cell on adsorption of CO_2. The K^+ cations in the 8-rings also shifted slighted off the mirror plane of the 8-ring. The peaks from the CO_2 molecules were not visible in this Fourier map because of the high X-ray scattering power of K^+. To determine the positions of CO_2 upon adsorption, new CO_2-Fourier maps were calculated using the in situ X-ray diffraction data under adsorption of CO_2 using a model with both framework and

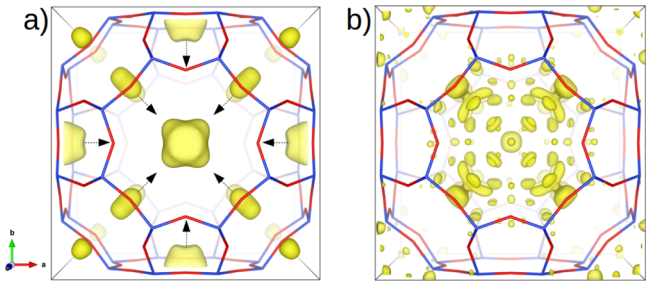

Figure 4. Difference Fourier maps (electron densities) of zeolite K-ZK-4. (a) Yellow areas in the map denote positions of the K^+ and CO_2 and the arrows show the cation shift and (b) yellow areas come from the randomly oriented CO_2 molecules during loading at 1.0 bar.

extraframework cations. In the map derived at the highest pressure of CO_2 (Figure 4b), the positioning of adsorbed CO_2 was described as rather randomly spread density peaks as is visible from the yellow areas in the map.

The Rietveld analysis of the X-ray diffraction data showed that the cation shifts during the adsorption of CO_2 were rather small, up to ~0.2 Å for the samples measured at 1 bar. The analysis also showed that the total number of K^+ was 6.7(1), which was close to the values derived from other techniques (see Table 2). For the data collected for different CO_2

Table 2. Synthesis Gel Composition for Zeolite Na-ZK-4 with Different Si/Al Ratios

	solution 1			solution 2	
Si/Al	$NaAlO_2$ (g)	NaOH (g)	H_2O (g)	TMAOH (g)	SiO_2 (HS-40) (g)
1.8	2.15	0.60	30	30	5.70
2.3	2.15	0.45	30	25	10.72
2.8	2.15	0.45	30	25	12.33

pressures, a number of CO_2 molecules per unit cell were obtained and were 1.7(1), 4.1(1), and 6.0(1) molecules at pressures of 0.1, 0.4, and 1 bar, respectively.

Molecular Details of the CO_2 Adsorption. To understand the mode of CO_2 adsorption on zeolite ZK-4, we monitored the adsorption of CO_2 on the selected zeolite ZK-4s using in situ infrared (IR) spectroscopy. Bands for both physisorbed and chemisorbed CO_2 were detected in the IR spectra in Figure 5. The relative fraction of chemisorbed CO_2 was higher on zeolite Na-ZK-4 (1.8) at low CO_2 pressures than that at high pressures. However, irrespectively of the pressure, the major mode of CO_2 adsorption was via physisorption, as derived from the very large intensity of the asymmetric stretching υ_3 band at around 2360 cm^{-1} (the band that appeared at 2289 cm^{-1} was related to $^{13}CO_2$).[45] The frequency of this band downshifted at increased loading of CO_2, which was consistent with that CO_2 adsorbed at high-energy sites at low loading of CO_2.[23,46] At very low CO_2 coverage, the physisorbed CO_2 occurred on the high-energy physisorption sites that are typically located close to the cations. CO_2 can interact with one or more cations if the cations are located close to each other there. We have previously investigated the effect of the cation on CO_2 physisorption by density functional theory (DFT) calculations for zeolite A and zeolite Na-ZK-4 (1.3). We observed that at low CO_2 coverage, different cations and their crystallographic sites can affect the orientation of the physisorbed CO_2. As zeolite Na-ZK-4 (1.8) shares the same

https://dx.doi.org/10.1021/acsomega.0c03749
ACS Omega 2020, 5, 25371−25380

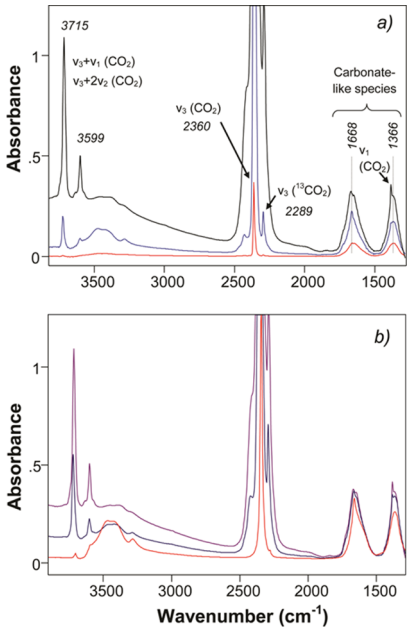

Figure 5. IR spectra of CO_2 adsorbed on zeolite Na-ZK-4 (Si/Al ~1.8:1) in (a) adsorption branch at CO_2 pressures of 6.7 Pa, 133 Pa, and 13.3 kPa (bottom to top) and (b) desorption branch at CO_2 pressures of 13.3 kPa, 667 Pa, and 20 min of evacuation under dynamic vacuum conditions.

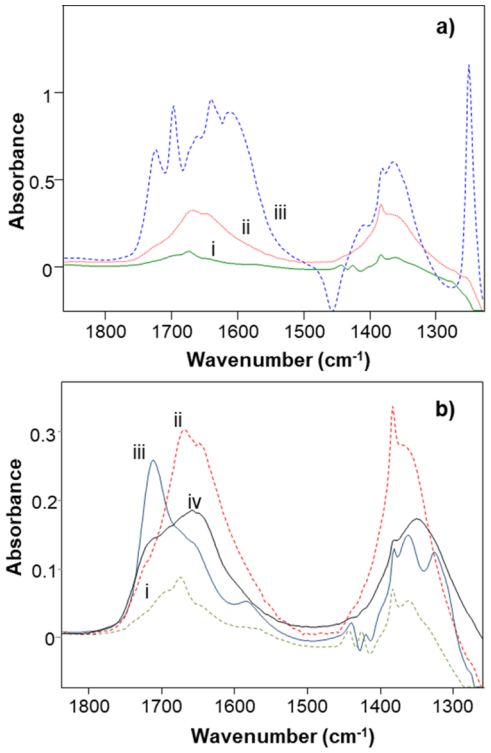

Figure 6. (a) IR spectra of (i) zeolites Na-ZK-4 (Si/Al = 2.8:1), (ii) Na-ZK-4 (Si/Al = 1.8:1), and (iii) NaA. The bands were assigned to carbonate and/or carbonate-like species, and there are more different kinds of such species in the case of zeolite 4A and (b) IR spectra of (i) zeolites Na-ZK-4 (Si/Al = 2.8:1), (ii) Na-ZK-4 (Si/Al = 1.8:1), (iii) NaK-ZK-4 (Si/Al = 2.8:1) 55 at. % K^+, and (iv) NaK-ZK-4 (1.8) 28 at. % K^+.

structure as zeolite A and zeolite Na-ZK-4 (1.3), we expect a similar behavior on CO_2 adsorbed on zeolite Na-ZK-4 (1.8).[23,26] Also, we have shown by in situ neutron diffraction studies that most of the CO_2 do indeed physisorb by bridging two cations in zeolite A.[24] In our previous studies, we also demonstrated using DFT calculations that the frequency of the υ_3 band can be shifted depending on the cation composition near the physisorbed CO_2. The high-frequency bands at 3599 and 3715 cm^{-1} were attributed to the combination of frequencies ($\upsilon_1 + \upsilon_3$ and $\upsilon_1 + 2\upsilon_2$) of physisorbed CO_2. The normally forbidden band for CO_2 (symmetric stretching υ_1 band at 1383 cm^{-1}) appeared at high loadings of CO_2 and informed on that sufficiently many CO_2 molecules had a distorted symmetry.

Although physisorption of CO_2 was dominant, chemisorption of CO_2 was still detectable and could be seen from the broad bands at 1668 and 1366 cm^{-1} (Figures 5 and 6), which were somewhat similar to the bands observed for chemisorption on zeolite A.[47−50] These bands, according to the split (~300 cm^{-1}) of double-degenerated carbonate bands, were assigned to bidentate carbonates.[48] As it is always very difficult to remove all the water from aluminum-rich zeolites, it is very well possible that some bicarbonates had formed upon CO_2 chemisorption.[36] The appearance of the broad OH bands at 3400 cm^{-1} on the spectra in Figure 5 can be a further indication of bicarbonate formation. The physisorbed CO_2 could be removed from the pores of zeolite Na-ZK-4 by evacuation, but the chemisorbed species remain in the zeolite (cf. Figure 6a). The fraction of chemisorbed CO_2 was the highest on zeolite Na-A and then successively lower on zeolites Na-ZK-4 (Si/Al ~ 1.8) and Na-ZK-4 (Si/Al ~ 2.8) (cf. Figures 5 and 6a), which was assigned to the decrease in the number of Al atoms and the metal cations that provided the basicity of the zeolites. The intensities of the chemisorption bands were lower compared with studies of zeolite A.[20,23,26] Because the amount of zeolites used to make the self-supporting pellets was roughly the same (~25 mg), the pellets had very similar thickness, and hence, a semiquantitative comparison was possible. It is important to note that apart from the number of Al atoms, the cations could also affect the chemisorption of CO_2 on these zeolites. K^+ is slightly less-electronegative than Na^+ (0.9 vs 0.8), and the K^+-containing zeolite ZK-4 would have higher basicity as compared with the pure Na^+ zeolite ZK-4. Figure 6b demonstrates clearly the effect on the chemisorption of CO_2 when introducing K^+ on Na-ZK-4 (Si/Al ~ 2.8). An increased intensity of the corresponding bands and shifts in the frequencies are observed in Figure 6b when comparing spectra (i) and (iii), displaying the increased degree of chemisorption of CO_2 when 55 at. % of the Na^+ was replaced with K^+ on Na-ZK-4 (Si/Al ~ 2.8). The split of some carbonate (or bicarbonate) bands also increased in magnitude from ~300 cm^{-1} on Na-ZK-4 (Si/Al ~ 2.8) to around 350 cm^{-1} on NaK-ZK-4 (Si/Al ~ 2.8) 55 at. % K^+. Similar increases in the magnitude of the split were observed when comparing Na-ZK-4 (Si/Al ~ 1.8) and NaK-ZK-4 (Si/Al ~ 1.8) 28 at. % K^+; however, no increased amount of chemisorbed CO_2 was observed on NaK-ZK-4 (Si/Al ~ 1.8) 28 at.% K^+.

Kinetics of CO_2 Sorption. We followed the physisorption of CO_2 by monitoring the development of the $\upsilon_1 + \upsilon_3$ and $\upsilon_1 + 2\upsilon_2$ combination band at 3317 cm^{-1} with respect to time on zeolites Na-ZK-4 (1.8 and 2.8), NaK-ZK-4 (1.8), 28 at. % K^+ (the sample with the highest CO_2 selectivity at Si/Al = 1.8), and NaK-ZK-4 (2.8), 55 at. % K^+ (the sample with the highest CO_2 selectivity at Si/Al = 2.8); see Figure 7. The zeolite Na-

https://dx.doi.org/10.1021/acsomega.0c03749
ACS Omega 2020, 5, 25371−25380

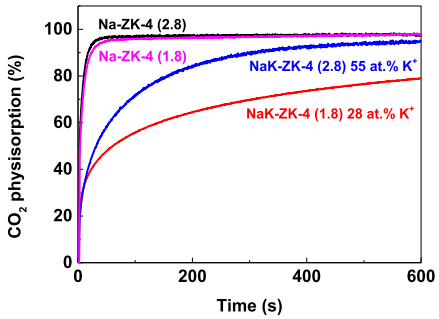

Figure 7. Kinetics of CO_2 physisorption on zeolites Na-ZK-4 (1.8, 2.8), NaK-ZK-4 (1.8) 28 at. %, and NaK-ZK-4 (2.8) 55 at. %.

ZK-4 (2.8) had the fastest uptake of CO_2, as shown in Figure 7, which was expected as it had only Na^+ ions, which made the passage of CO_2 more easy than that if K^+ ions were present. The physisorption of CO_2 on zeolite Na-ZK-4 (2.8) reached 60% of its maximum capacity already after 10 s. In the other two samples, the reduced CO_2 physisorption rates were due to K^+ ions populating the 8-rings. Specifically, zeolite NaK-ZK-4 (1.8) with 28 at. % of K^+ had the slowest uptake of CO_2, which took 10 min to reach 80% of its maximum CO_2 physisorption capacity (i.e., after 24 h). This slow uptake rate was related to that K^+ ions were present in the 8-rings of this zeolite and that the 6-rings were populated by Na^+ and K^+ ions. The CO_2 adsorbing more rapidly on zeolite NaK-ZK-4 (2.8) 55 at. % than on zeolite NaK-ZK-4 (1.8) 28. at. % was ascribed to the smaller amount of Na^+ and K^+ cations in the 6-rings in the zeolite with a Si/Al ratio of 2.8.

The trend of a maximum CO_2-over-N_2 selectivity for zeolites NaK ZK-4 at intermediate K^+ contents was also preliminarily investigated by molecular dynamics simulations for comparison (detailed in the Supporting Information). From these calculations, it was estimated that the diffusivities of N_2 in zeolite NaK-ZK-4 (2.3) had a minimum at intermediate K^+ contents, which supports that the estimated high CO_2-over-N_2 selectivity was related to a kinetic enhancement of the selectivity by a reduced diffusion of N_2 throughout the pores of zeolite NaK ZK-4 (see Table S2 for the calculated diffusivities).

CONCLUSIONS

Zeolite NaK-ZK-4 with Si/Al = 1.8−2.8 and intermediate numbers of K^+ cations had very high CO_2 selectivity and good levels of CO_2 uptake. The high selectivity was ascribed to the presence of K^+ cations close to the edge of the 8-ring and Na^+ cations in the 6-rings of the zeolite that blocked the adsorption/diffusion of N_2. The CO_2 uptake kinetics of the highly selective zeolite NaK-ZK-4s was slower than that of the Na-ZK-4s without any K^+ cations. On the other hand, the highly selective compositions of zeolite NaK-ZK-4 with a high Si/Al ratio (2.8) showed a faster CO_2 adsorption kinetics than the equally selective zeolite NaK-ZK-4 with a low Si/Al ratio (1.8). Further studies of the crystallography and temperature dependency of the CO_2 selectivity could be motivated for this and related 8-ring zeolites. Compositions with even less aluminum than zeolite NaK ZK-4 (2.8) could be advantageous toward real applications for CO_2 capture by assuring fast uptake and somewhat reduced hydrophilicity.

EXPERIMENTAL SECTION

Synthesis and Characterization. Zeolites Na-ZK-4 with Si/Al = 1.8, 2.3, and 2.8 were synthesized via a hydrothermal method further developed from our previous work.[26] A typical synthesis involved making two separate mixtures. The first mixture contained sodium aluminate and sodium hydroxide in deionized water. The second mixture contained colloidal silica (HS-40) and tetramethylammonium hydroxide (TMAOH—20% in H_2O) solution. The two mixtures were agitated for 30 min and then combined together. The final mixture was agitated for a further 120 min and then left to age for 24 h at room temperature (RT). The aged reaction gel was transferred to a Teflon-lined stainless-steel autoclave and heated up to 373 K between 20 and 72 h. The appropriate amounts of each substance and their resulting Si/Al ratios are listed in Table 2. (We noted the cocrystallization of zeolite Y when the amount of colloidal silica was increased relative to $NaAlO_2$). The as-synthesized zeolite Na-ZK-4 was calcined at 773 K for 24 h to remove the organic template. Powder XRD patterns for zeolite Na-ZK-4 samples and two scanning electron microscopy images are presented in Figures S1−S5. Ion exchange of zeolite Na-ZK-4 to NaK-ZK-4 and K-ZK-4 was carried out using the same procedures as published by Liu et al.[20] In the rest of this study, zeolite ZK-4 with Si/Al = 1.8, 2.3, and 2.8 will be denoted as zeolites ZK-4 (1.8), ZK-4 (2.3), and ZK-4 (2.8), respectively. Zeolite ZK-4 (1.8) with only Na^+ exchangeable cations would be written as "zeolite Na-ZK-4 (1.8)". Zeolite ZK-4 (1.8) with both Na^+ and K^+, and the amount of K^+ cations being 50 at. % of the total number of exchangeable cations, will be presented as "zeolite NaK-ZK-4 (1.8) (K^+ = 50 at. %)".

Inductively coupled plasma−optical emission spectrometry (ICP−OES) was used to determine the concentration of K^+/Na^+/Si/Al in the zeolite K-ZK-4 samples. The error range for the ICP−OES was in the ppm region, and these experiments were performed by MEDAC Ltd., Surrey, UK.

Gas Adsorption Analysis. CO_2 and N_2 gas adsorption/desorption isotherms were recorded using a Micromeritics ASAP 2020 surface area analyzer at pressures of 0−101 kPa. The samples were prepared by heating to 623 K under high dynamic vacuum (1×10^{-4} Pa) for 6 h. The N_2 uptake at 77 K was determined using a liquid N_2 bath as the temperature control medium. Gas adsorption measurements at 273 K were carried out using an ice slurry bath to keep the temperature constant. Gas adsorption measurements at ambient temperatures (283−303 K) were carried out using a Julabo CF-31 temperature control unit for temperature control.

CO_2 physisorption isotherms were obtained for all tested samples at 273, 283, 293, and 303 K. This was achieved by recording two sets of CO_2 adsorption isotherms on a freshly prepared (heat treated) sample with only a 5 min vacuum regeneration at RT in between. The second adsorption isotherm is considered as the CO_2 physisorption isotherms as any possible chemisorbed CO_2 would not have been removed during the vacuum regeneration. The rate of CO_2 physisorption presented in the Supporting Information (Figure S6) was determined using the rate of adsorption addon of the Micromeritics ASAP software and the data were obtained during the second CO_2 adsorption cycle at 273 K. The isosteric heat of CO_2 physisorption was modeled using the CO_2 physisorption isotherms recorded at 273, 283, 293, and 303 K using the Clausius−Clapeyron equation.

https://dx.doi.org/10.1021/acsomega.0c03749
ACS Omega 2020, 5, 25371−25380

For all the adsorption/desorption isotherms, the adsorption/desorption points were determined when the pressure change in the system had dropped to below 0.01% over a period of 10 s (with an initial delay of 100 s). A longer equilibration time (30 s, with 300 s delay) was also tested; there was a minimal difference to the quality of the recorded data, which was also shown previously in zeolite ZK-4 (1.3).[26] Even if the recorded isotherms may not be true equilibrium isotherms, they are nevertheless representative for the zeolites.

The binary gas selectivity on adsorbents can be estimated from single-component adsorption data in several manners, and in this study, we used the method based on dividing the corresponding Henry's law coefficients in dilution.

IR Spectroscopy. The IR spectra were recorded on a Varian 670-IR FT-IR spectrometer using a mercury cadmium telluride detector, which was cooled with liquid N_2. The in situ experiments were performed with a high-vacuum stainless-steel manifold connected to a stainless-steel IR transmission cell. Samples of zeolite ZK-4 (~25 mg) were pressed into pellets with a pressure of 1×10^9 kg/m^2 for 2 min. The pellets were heated to 523 K under high dynamic vacuum ($<1 \times 10^{-4}$ Pa) in the IR cell for a minimum of 6 h before the in situ measurements were performed. After degassing of the zeolite pellet, CO_2 was let into the IR cell and spectra were recorded as a function of the CO_2 pressure and time. A detailed description of the experimental approach has been presented previously.[8,23]

The physisorption rate was measured by in situ IR spectroscopy by the combination band ($\upsilon_1 + \upsilon_3$ or $\upsilon_3 + 2\upsilon_2$) at 3317 cm^{-1}. The regular υ_3 band had too high intensity, became saturated, and did not obey the Lambert–Beer law even at relatively low pressures of CO_2. The pretreated zeolite was subjected to 13.3 kPa of CO_2, and the development of the combination band was monitored with respect to CO_2 exposure time. The intensity of the band was normalized against the equilibrium intensity (recorded when there were no noticeable changes with the intensity of the band but with a minimum delay of 24 h).

X-ray Diffraction. XRD data for the high-silica zeolite K-ZK-4 (2.8) at different loadings of CO_2 were collected on a beamline ID-22 at the European Synchrotron Radiation Facility (ESRF) in Grenoble, France. These in situ measurements, involving a gas cell, were performed with a wavelength of 0.4 Å, covering the 2θ range of 1.7–25°. Prior to the diffraction measurements, the powder samples were loaded into borosilicate capillaries with a diameter of 0.7 mm and then glued to the gas cell. The measurements were repeated in three steps for each sample at different pressures of CO_2: (i) a preliminary scan with the as-prepared sample (hydrated) at RT, (ii) a second scan with the sample being dehydrated for 30 min at 250 °C under dynamic vacuum, and (iii) a third scan performed at the desired pressure of CO_2 after the sample had been cooled down to RT. The crystal structure of zeolite K-ZK-4 (2.8) was studied for four different pressures of CO_2: 0, 10, 40, and 101 kPa at RT. For each gas pressure, a new capillary was used. The Rietveld analysis of the XRPD data was performed with the TOPAS 4 program,[51] and the difference Fourier maps were generated using the GSAS package[52] and the Foue program.[53]

■ ASSOCIATED CONTENT

Supporting Information

The Supporting Information is available free of charge at https://pubs.acs.org/doi/10.1021/acsomega.0c03749.

Additional adsorption isotherms, powder X-ray diffractograms, scanning electron microscopy images, and further information on experimental methods (PDF)

■ AUTHOR INFORMATION

Corresponding Author

Niklas Hedin − *Department of Materials and Environmental Chemistry, Arrhenius Laboratory, Stockholm University, Stockholm SE 106 91, Sweden;* orcid.org/0000-0002-7284-2974; Email: niklas.hedin@mmk.su.se

Authors

Ocean Cheung − *Department of Materials and Environmental Chemistry, Arrhenius Laboratory, Stockholm University, Stockholm SE 106 91, Sweden; Nanotechnology and Functional Materials, Department of Materials Science and Engineering, Uppsala University, Uppsala SE 75121, Sweden;* orcid.org/0000-0002-4072-4324

Zoltán Bacsik − *Department of Materials and Environmental Chemistry, Arrhenius Laboratory, Stockholm University, Stockholm SE 106 91, Sweden*

Nicolas Fil − *Department of Materials and Environmental Chemistry, Arrhenius Laboratory, Stockholm University, Stockholm SE 106 91, Sweden*

Panagiotis Krokidas − *Department of Materials and Environmental Chemistry, Arrhenius Laboratory, Stockholm University, Stockholm SE 106 91, Sweden; Institute of Nanoscience and Nanotechnology, National Centre for Scientific Research "Demokritos", Athens GR-15310, Greece*

Dariusz Wardecki − *Department of Materials and Environmental Chemistry, Arrhenius Laboratory, Stockholm University, Stockholm SE 106 91, Sweden; Department of Chemistry and Chemical Engineering, Chalmers University of Technology, Gothenburg SE 412 96, Sweden; Institute of Experimental Physics, Faculty of Physics, University of Warsaw, Warsaw 02-093, Poland*

Complete contact information is available at: https://pubs.acs.org/10.1021/acsomega.0c03749

Notes

The authors declare no competing financial interest.

■ ACKNOWLEDGMENTS

We thank Professor Xiaodong Zou for sharing her beamtime with us. The Berzelii Center EXSELENT funded by partners, VINNOVA and the Swedish Research Council, is acknowledged.

■ REFERENCES

(1) Ekins, P.; Pye, S.; Winning, M.; Macrory, R.; Milligan, B.; Haszeldine, S.; Watson, J. *The Role of CCS in Meeting Climate Policy Targets*; Global CCS Institute, 2017.

(2) Rubin, E. S.; Mantripragada, H.; Marks, A.; Versteeg, P.; Kitchin, J. The Outlook for Improved Carbon Capture Technology. *Prog. Energy Combust. Sci.* **2012**, *38*, 630–671.

(3) Hedin, N.; Andersson, L.; Bergström, L.; Yan, J. Adsorbents for the Post-Combustion Capture of CO_2 Using Rapid Temperature Swing or Vacuum Swing Adsorption. *Appl. Energy* **2013**, *104*, 418–433.

(4) Lee, S.-Y.; Park, S.-J. A Review on Solid Adsorbents for Carbon Dioxide Capture. *J. Ind. Eng. Chem.* **2015**, *23*, 1−11.
(5) Lashaki, M. J.; Khiavi, S.; Sayari, A. Stability of Amine-Functionalized CO_2 Adsorbents: A Multifaceted Puzzle. *Chem. Soc. Rev.* **2019**, *48*, 3320−3405.
(6) Siriwardane, R. V.; Shen, M.-S.; Fisher, E. P.; Losch, J. Adsorption of CO_2 on Zeolites at Moderate Temperatures. *Energy Fuels* **2005**, *19*, 1153−1159.
(7) Creamer, A. E.; Gao, B. Carbon-Based Adsorbents for Postcombustion CO_2 Capture: A Critical Review. *Environ. Sci. Technol.* **2016**, *50*, 7276−7289.
(8) Cheung, O.; Liu, Q.; Bacsik, Z.; Hedin, N. Silicoaluminophosphates as CO2 Sorbents. *Microporous Mesoporous Mater.* **2012**, *156*, 90−96.
(9) Liu, Q.; Cheung, N. C. O.; Garcia-Bennett, A. E.; Hedin, N. Aluminophosphates for CO_2 Separation. *ChemSusChem* **2011**, *4*, 91−97.
(10) Yu, J.; Xie, L.-H.; Li, J.-R.; Ma, Y.; Seminario, J. M.; Balbuena, P. B. CO2 Capture and Separations Using MOFs: Computational and Experimental Studies. *Chem. Rev.* **2017**, *117*, 9674−9754.
(11) Dunne, J. A.; Mariwala, R.; Rao, M.; Sircar, S.; Gorte, R. J.; Myers, A. L. Calorimetric Heats of Adsorption and Adsorption Isotherms. 1. O_2, N_2, Ar, CO_2, CH_4, C_2H_6 and SF_6 on Silicalite. *Langmuir* **1996**, *12*, 5888−5895.
(12) Walton, K. S.; Abney, M. B.; Douglas LeVan, M. CO_2 Adsorption in Y and X Zeolites Modified by Alkali Metal Cation Exchange. *Microporous Mesoporous Mater.* **2006**, *91*, 78−84.
(13) Bae, T.-H.; Hudson, M. R.; Mason, J. A.; Queen, W. L.; Dutton, J. J.; Sumida, K.; Micklash, K. J.; Kaye, S. S.; Brown, C. M.; Long, J. R. Evaluation of Cation-Exchanged Zeolite Adsorbents for Post-Combustion Carbon Dioxide Capture. *Energy Environ. Sci.* **2013**, *6*, 128−138.
(14) Guo, X.; Corbin, D. R.; Navrotsky, A. Thermodynamics of H_2O and CO_2 Absorption and Guest-Induced Phase Transitions in Zeolite RHO. *J. Phys. Chem. C* **2018**, *122*, 20366−20376.
(15) Lozinska, M. M.; Mangano, E.; Greenaway, A. G.; Fletcher, R.; Thompson, S. P.; Murray, C. A.; Brandani, S.; Wright, P. A. Cation Control of Molecular Sieving by Flexible Li-Containing Zeolite Rho. *J. Phys. Chem. C* **2016**, *120*, 19652−19662.
(16) Shang, J.; Li, G.; Singh, R.; Gu, Q.; Nairn, K. M.; Bastow, T. J.; Medhekar, N.; Doherty, C. M.; Hill, A. J.; Liu, J. Z.; Webley, P. A. Discriminative Separation of Gases by a "Molecular Trapdoor" Mechanism in Chabazite Zeolites. *J. Am. Chem. Soc.* **2012**, *134*, 19246−19253.
(17) Zhao, J.; Xie, K.; Singh, R.; Xiao, G.; Gu, Q.; Zhao, Q.; Li, G.; Xiao, P.; Webley, P. A. Li+/ZSM-25 Zeolite as a CO_2 Capture Adsorbent with High Selectivity and Improved Adsorption Kinetics, Showing CO_2-Induced Framework Expansion. *J. Phys. Chem. C* **2018**, *122*, 18933−18941.
(18) Grande, C. A.; Blom, R. Cryogenic Adsorption of Methane and Carbon Dioxide on Zeolites 4A and 13X. *Energy Fuels* **2014**, *28*, 6688−6693.
(19) Jaramillo, E.; Chandross, M. Adsorption of Small Molecules in LTA Zeolites. 1. NH3, CO2, and H2O in Zeolite 4A. *J. Phys. Chem. B* **2004**, *108*, 20155−20159.
(20) Liu, Q.; Mace, A.; Bacsik, Z.; Sun, J.; Laaksonen, A.; Hedin, N. NaKA Sorbents with High CO_2-over-N_2 Selectivity and High Capacity to Adsorb CO_2. *Chem. Commun.* **2010**, *46*, 4502.
(21) Liu, Z.; Grande, C. A.; Li, P.; Yu, J.; Rodrigues, A. E. Adsorption and Desorption of Carbon Dioxide and Nitrogen on Zeolite 5A. *Sep. Sci. Technol.* **2011**, *46*, 434−451.
(22) Akhtar, F.; Liu, Q.; Hedin, N.; Bergström, L. Strong and Binder Free Structured Zeolite Sorbents with Very High CO_2-over-N_2 Selectivities and High Capacities to Adsorb CO_2 Rapidly. *Energy Environ. Sci.* **2012**, *5*, 7664.
(23) Cheung, O.; Bacsik, Z.; Liu, Q.; Mace, A.; Hedin, N. Adsorption Kinetics for CO_2 on Highly Selective Zeolites NaKA and Nano-NaKA. *Appl. Energy* **2013**, *112*, 1326−1336.
(24) Rzepka, P.; Bacsik, Z.; Smeets, S.; Hansen, T. C.; Hedin, N.; Wardecki, D. Site-Specific Adsorption of CO_2 in Zeolite NaK-A. *J. Phys. Chem. C* **2018**, *122*, 27005−27015.
(25) Rzepka, P.; Wardecki, D.; Smeets, S.; Müller, M.; Gies, H.; Zou, X.; Hedin, N. CO_2-Induced Displacement of Na+ and K+ in Zeolite | NaKl-A. *J. Phys. Chem. C* **2018**, *122*, 17211−17220.
(26) Cheung, O.; Bacsik, Z.; Krokidas, P.; Mace, A.; Laaksonen, A.; Hedin, N. K+ Exchanged Zeolite ZK-4 as a Highly Selective Sorbent for CO_2. *Langmuir* **2014**, *30*, 9682−9690.
(27) Pham, T. D.; Hudson, M. R.; Brown, C. M.; Lobo, R. F. Molecular Basis for the High CO_2 Adsorption Capacity of Chabazite Zeolites. *ChemSusChem* **2014**, *7*, 3031−3038.
(28) Zhang, J.; Singh, R.; Webley, P. A. Alkali and Alkaline-Earth Cation Exchanged Chabazite Zeolites for Adsorption Based CO_2 Capture. *Microporous Mesoporous Mater.* **2008**, *111*, 478−487.
(29) Liu, Q.; Pham, T.; Porosoff, M. D.; Lobo, R. F. ZK-5: A CO_2-Selective Zeolite with High Working Capacity at Ambient Temperature and Pressure. *ChemSusChem* **2012**, *5*, 2237−2242.
(30) Lozinska, M. M.; Mowat, J. P. S.; Wright, P. A.; Thompson, S. P.; Jorda, J. L.; Palomino, M.; Valencia, S.; Rey, F. Cation Gating and Relocation during the Highly Selective "Trapdoor" Adsorption of CO_2 on Univalent Cation Forms of Zeolite Rho. *Chem. Mater.* **2014**, *26*, 2052−2061.
(31) Min, J. G.; Kemp, K. C.; Hong, S. B. Zeolites ZSM-25 and PST-20: Selective Carbon Dioxide Adsorbents at High Pressures. *J. Phys. Chem. C* **2017**, *121*, 3404−3409.
(32) Hudson, M. R.; Queen, W. L.; Mason, J. A.; Fickel, D. W.; Lobo, R. F.; Brown, C. M. Unconventional, Highly Selective CO_2 Adsorption in Zeolite SSZ-13. *J. Am. Chem. Soc.* **2012**, *134*, 1970−1973.
(33) Pham, T. D.; Lobo, R. F. Adsorption Equilibria of CO_2 and Small Hydrocarbons in AEI-, CHA-, STT-, and RRO-Type Siliceous Zeolites. *Microporous Mesoporous Mater.* **2016**, *236*, 100−108.
(34) Cheetham, A. K.; Eddy, M. M.; Klinowski, J.; Thomas, J. M. A Study of Si, Al Ordering and Cation Positions in the Zeolites Sodium ZK-4 and Sodium Y by Neutron Diffraction. *J. Chem. Soc., Chem. Commun.* **1983**, *1*, 23−25.
(35) Eddy, M. M.; Cheetham, A. K.; David, W. I. F. Powder Neutron Diffraction Study of Zeolite Na-ZK-4; an Application of New Functions for Peak Shape and Asymmetry. *Zeolites* **1986**, *6*, 449−454.
(36) Rzepka, P.; Bacsik, Z.; Pell, A. J.; Hedin, N.; Jaworski, A. Nature of Chemisorbed CO_2 in Zeolite A. *J. Phys. Chem. C* **2019**, *123*, 21497−21503.
(37) Lin, L.-C.; Berger, A. H.; Martin, R. L.; Kim, J.; Swisher, J. A.; Jariwala, K.; Rycroft, C. H.; Bhown, A. S.; Deem, M. W.; Haranczyk, M.; Smit, B. In Silico Screening of Carbon-Capture Materials. *Nat. Mater.* **2012**, *11*, 633−641.
(38) Ikeda, T.; Kodaira, T.; Oh, T.; Nisawa, A. K^+ Ion Distribution in Zeolite ZK-4's with Various Si/Al Ratios and the Contribution of K^+ Ions to K Cluster Formation. *Microporous Mesoporous Mater.* **2003**, *57*, 249−261.
(39) Sircar, S. Influence of Adsorbate Size and Adsorbent Heterogeneity of IAST. *AIChE J.* **1995**, *41*, 1135−1145.
(40) Björnerbäck, F.; Bernin, D.; Hedin, N. Microporous Humins Synthesized in Concentrated Sulfuric Acid Using 5-Hydroxymethyl Furfural. *ACS Omega* **2018**, *3*, 8537−8545.
(41) Pluth, J. J.; Smith, J. V. Accurate Redetermination of Crystal Structure of Dehydrated Zeolite A. Absence of near Zero Coordination of Sodium. Refinement of Si,Al-Ordered Superstructure. *J. Am. Chem. Soc.* **1980**, *102*, 4704−4708.
(42) Cornelius, M.-L. U.; Price, L.; Wells, S. A.; Petrik, L. F.; Sartbaeva, A. The Steric Influence of Extra-Framework Cations on Framework Flexibility: An LTA Case Study. *Z. Kristallogr. - Cryst. Mater.* **2019**, *234*, 461−468.
(43) Coudert, F.-X.; Kohen, D. Molecular Insight into CO_2 "Trapdoor" Adsorption in Zeolite Na-RHO. *Chem. Mater.* **2017**, *29*, 2724−2730.
(44) Cheung, O.; Wardecki, D.; Bacsik, Z.; Vasiliev, P.; McCusker, L. B.; Hedin, N. Highly Selective Uptake of Carbon Dioxide on the

https://dx.doi.org/10.1021/acsomega.0c03749
ACS Omega 2020, 5, 25371−25380

Zeolite |na10.2KCs0.8|- LTA -a Possible Sorbent for Biogas Upgrading. *Phys. Chem. Chem. Phys.* **2016**, *18*, 16080−16083.
(45) Pirngruber, G. D.; Raybaud, P.; Belmabkhout, Y.; Čejka, J.; Zukal, A. The Role of the Extra-Framework Cations in the Adsorption of CO_2 on Faujasite Y. *Phys. Chem. Chem. Phys.* **2010**, *12*, 13534.
(46) Delaval, Y.; de Lara, E. C. Study of Physisorption of Carbon Dioxide on NaA Zeolite. Part 2. - Interpretation of Infrared Spectra from Statistical Models. *J. Chem. Soc., Faraday Trans. 1* **1981**, *77*, 879.
(47) Busca, G. Acidity and Basicity of Zeolites: A Fundamental Approach. *Microporous Mesoporous Mater.* **2017**, *254*, 3−16.
(48) Busca, G.; Lorenzelli, V. Infrared Spectroscopic Identification of Species Arising from Reactive Adsorption of Carbon Oxides on Metal Oxide Surfaces. *Mater. Chem.* **1982**, *7*, 89−126.
(49) Masuda, T.; Tsutsumi, K.; Takahashi, H. Infrared and Calorimetric Studies of Adsorbed Carbon Dioxide on NaA and CaNaA Zeolites. *J. Colloid Interface Sci.* **1980**, *77*, 232−237.
(50) Montanari, T.; Busca, G. On the Mechanism of Adsorption and Separation of CO_2 on LTA Zeolites: An IR Investigation. *Vib. Spectrosc.* **2008**, *46*, 45−51.
(51) Coelho, A. A. TOPAS and TOPAS-Academic: An Optimization Program Integrating Computer Algebra and Crystallographic Objects Written in C++. *J. Appl. Crystallogr.* **2018**, *51*, 210−218.
(52) Larson, A. C.; Von Dreele, R. B. *General Structure Analysis System (GSAS)*, Los Alamos National Laboratory Report LAUR 86-748, 2004.
(53) Belmonte, S. A. *FOUE*, 2000.

https://dx.doi.org/10.1021/acsomega.0c03749
ACS Omega 2020, 5, 25371−25380